Co-published by
Institute of Fluid-Flow Machinery
Polish Academy of Sciences
Committee on Thermodynamics and Combustion
Polish Academy of Sciences

http://www.imp.gda.pl/archives-of-thermodynamics/

Experimental investigation into the influence of heat source power on the performance of a scroll expander in an organic Rankine cycle system using HFE-7100 fluid

Tomasz Zygmunt Kaczmarczyk

Institute of Fluid Flow Machinery, Polish Academy of Sciences, Fiszera 14, 80-231 Gdańsk, Poland
Author email: tkaczmarczyk@imp.gda.pl

Received: 17.07.2025; revised: 04.12.2025; accepted: 23.01.2026

Abstract

This work presents the results of an experimental study on a 1 kW scroll expander in an organic Rankine cycle (ORC) system. The low-boiling, non-flammable hydrofluoroether HFE-7100, was used as the working fluid. The research was conducted at heat source power levels ranging from 10 kW_t to 18 kW_t. The flow rate of the working medium was in the range of 30 g/s to 60 g/s. The generator of the expansion unit, on the other hand, was loaded with electrical receivers, with a load ranging from 200 W_e to 2000 W_e. The study shows that, for the same working fluid flow rate and expander rotational speed, an increase in the thermal power of the heat source resulted in higher voltage at the generator terminals and increased electrical output power of the ORC system. It was found that, regardless of the HFE-7100 flow rate, the inclination angles of the electrical power and voltage curves with respect to the expander's rotational speed axis increased as the thermal power of the heat source increased. Thus, for each level of a thermal power, there is an optimum generator load at which the electrical output power of the system is maximised. The research conducted shows that the maximum electrical output of 635 W_e was obtained for a heat source power of 16 kW_t and a fluid flow rate of 60 g/s. In addition, it was found that for the tested ranges of heat source power and HFE-7100 flow rate, the optimum load for the expander generator was between 3.5 Ω and 4.8 Ω.

Keywords: Scroll expander; Heat source; ORC system, HFE-7100; Experimental research

Vol. 47(2026), No. 1, 125–136; doi: 10.24425/ather.2026.158664

Cite this manuscript as: Kaczmarczyk, T.Z. (2026). Experimental investigation into the influence of heat source power on the performance of a scroll expander in an organic Rankine cycle system using HFE-7100 fluid. *Archives of Thermodynamics*, 47(1), 125–136.

1. Introduction

The need to move away from the exploitation of fossil fuels [1] necessitates the use of low-carbon fuel cells [2,3], the development of new environmentally friendly energy technologies [4], the decentralisation of power generation [5] and the utilisation of biofuels and unconventional fuels [6]. Therefore, technologies that enable integration with renewable energy sources (RES) are of considerable interest [7]. One such technology that meets the above requirements is the organic Rankine cycle (ORC) system [8]. ORC systems can be powered not only by RES (e.g. biomass [9] or solar energy [10]). These systems can be supplied with low- [11], medium- [12] and high-temperature [13] waste heat [14]. The utilisation of waste heat to generate electricity [15] increases the operational efficiency of these systems [16]. The literature indicates that ORC systems are associated with energy storage [17], air storage [18] and thermal energy storage (TES) systems [19], nuclear power systems [20], refrigeration systems [21,22], trilateral flash cycle (TFC) systems [23], partial evaporator–organic Rankine cycle (PE-ORC) systems [24], organic Rankine cycle–vapour compression cycle (ORC-VCC) systems [25]; as well as engines, including gas engines (GEs) [26], internal combustion engines (ICEs) [27], thermal engines [28] and direct-fired hot water boilers [29].

Nomenclature

I – current, A
m – mass flow rate, kg/s
n – rotational speed, rpm
N – power, W
p – pressure, kPa
PR – pressure ratio
R – resistance, Ω
T – temperature, °C
U – voltage, V
x – vapour quality

Subscripts and Superscripts
e – electrical
t – thermal

Abbreviations and Acronyms
AC – alternating current
DC – direct current
ORC – organic Rankine cycle
RES – renewable energy sources
TES – thermal energy storage
WHR– waste heat recovery

Hence, theoretical analyses [30] and experimental studies of complete ORC systems or their components [31−33] are conducted to improve their operating efficiency [34]. Volumetric expanders [35,36] and flow expanders [37] are used in ORC systems. Flow expanders include Tesla turbines [38], radial inflow turbines [39], axial turbines [40], radial outflow turbines [41], radial-axial turbines [42], or combinations thereof [43]. Turbines are built as either single-stage [44] or multi-stage [45] units, which can be manufactured as partial admission turbines [46]. The literature indicates that research [47] and optimisation work are being carried out on turbines, such as blade [48,49] and nozzle [50,51] shape optimisation, with a focus on thermodynamic cycle efficiency [52] and mechanical aspects, such as rotor vibrations [53].

In contrast, the most commonly used volumetric expansion units include Wankel expanders [54], scroll expanders [55], Stirling engines [56], vane expanders [36], screw expanders [57] and reciprocating engines [58]. Volumetric expansion units are often analysed and studied in parallel [59] or in series [60] operation within ORC systems. Pumps [61] used in the working medium cycle are also the subject of investigation, owing to their significant influence on the back work ratio [62]. New working fluids (fourth-generation refrigerants) [63] are also being analysed and studied [64] in terms of thermal stability [65] and ORC system efficiency [66]. Expanders are tested mechanically [67] or electrically [68] to determine, among other factors, their efficiency.

For example, a study by Murthy et al. [69] found that the efficiency of a four-intersecting-vane expander prototype, operating in an ORC system with R134a as the working fluid, was approximately 35%. The electrical output power and the rotational speed of the expander were approximately 33 W and 500 rpm, respectively. A similar efficiency of approximately 36% was achieved by an axial turbine operating in an ORC system with R1233zde as the working fluid [70]. In contrast, the microturbine's rotational speed and electrical power were 8000 rpm and 812 W, respectively. The recorded thermal efficiency of the ORC system was 2.15%. As the electrical power of the expander increases, the thermal efficiency of the ORC system also increases. Research on the scroll expander using HFE-7100 fluid showed that, at an electrical power output of approximately 980 W, the efficiency of the expander and the thermal efficiency of the ORC system were 49.3% and approximately 3%, respectively. In contrast, research conducted on a scroll expander by Sun et al. [71] indicates that the maximum thermal efficiency of the ORC system and the shaft power were approximately 6.4% and 1.8 kW, respectively.

This paper presents the results of an experimental study of a scroll expander with a rated power of 1 kW_e, using the low-boiling fluid HFE-7100. The study was conducted parametrically, based on the heat source power, working fluid flow rate and electrical load of the scroll expander generator. The parametric current-voltage characteristic curves of the expansion unit address a clear gap in the existing research and literature. The novelty of this work lies in the interpolation of the test results based on the inclination angles of the lines representing electrical power and voltage with respect to the expander's rotational speed axis. Based on the study conducted, a methodology is presented for estimating the optimum load of the expander generator, depending on the heat source power and the flow rate of the low-boiling fluid. The generalised conclusions will allow the research findings to be used by a wide range of readers for both practical and theoretical purposes.

2. Experimental test stand

Research on a scroll expander with a rated power of 1 kW_e was carried out in an ORC system using the low-boiling fluid HFE-7100. The tested expansion unit, comprising a generator and a scroll expander connected by a clutch, is a commercial product manufactured by Air Squared. The technical data for the scroll expander and the generator are provided in Table 1.

Table 1. Technical parameters of the expansion unit components [60].

Parameter	Unit	Value
Scroll expander		
Model	–	E15H22N4.25
Nominal power	kW	1.0
Maximum pressure	kPa	1380
Displacement	cm^3/rev.	12
Maximum speed	rpm	3600
Maximum inlet temperature	°C	175
Expansion ratio	–	3.5
Generator		
Model	–	AB30L
Rated power	kW	2.4
Maximum rotational speed	rpm	3000
Rated voltage	V	240
Maximum current	A	10

Hydrofluoroether HFE-7100 was used as the working fluid in the ORC system. The fluid was selected based on thermodynamic and energy considerations, taking into account the environmental and safety factors. HFE-7100 is a dry fluid (as shown by the saturated liquid-vapour curve in Fig. 1), which helps prevent erosion of the flow components of the expansion unit. Its boiling point is approximately 61°C at atmospheric pressure. HFE-7100 is a non-flammable, non-explosive, non-mutagenic and non-toxic fluid. It has an ozone depletion potential (ODP) of zero. Selected thermodynamic properties of the HFE-7100 fluid are provided in Table 2.

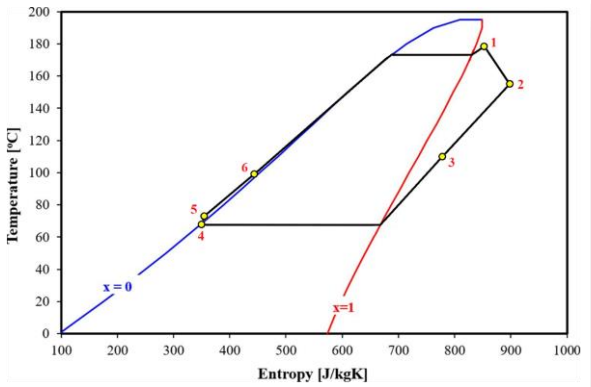

Fig. 1. Temperature-entropy (*T-s*) diagram of the test cycle with the scroll expander unit; *x* – vapour quality.

Table 2. Properties of HFE-7100 fluid at 25℃ [72].

Property	Value	Unit
Molecular weight	250	g/mol
Boiling point	61	°C
Critical temperature	195	°C
Critical pressure	2.23	MPa
Liquid density	1510	kg/m^3
Surface tension	13.6	mN/m
Dynamic viscosity	0.61	mPa s
Heat of vaporisation	112	kJ/kg
Vapour pressure	27.0	kPa
Coefficient of expansion	0.0018	1/K
Kinematic viscosity	0.38	cSt
Absolute viscosity	0.58	cP
Specific heat	1183	J/(kg K)
Thermal conductivity	0.069	W/(m K)

Fig. 2. Test stand used for testing a 1 kW scroll expander: 1 – scroll expander, 2 – generator, 3 – clutch, 4 – system for measuring pressure and temperature at the expander inlet, 5 – system for measuring pressure and temperature at the expander outlet, 6 – converter system, 7 – resistive load system, 8 – heat exchanger unit.

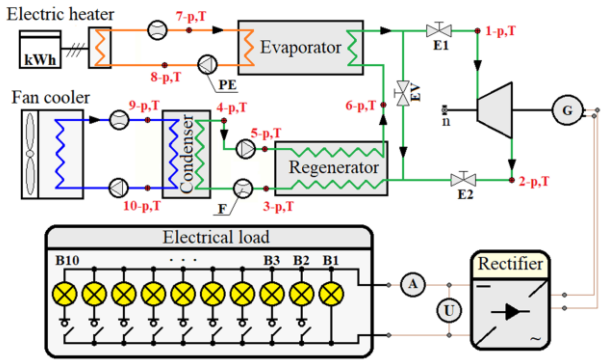

Fig. 3. Measurement diagram of the ORC system with a 1 kW scroll expander: PE – pumping engine, F – flowmeter, n – rotational speed measurement system, EV – expansion valve, E1 and E2 – valves at the expander's inlet and outlet, B(1–10) – electrical bulb, A – ammeter, U – voltmeter, G – generator, T – temperature measurement, p – pressure measurement, 1–10 – state points.

A photograph of the ORC system is shown in Fig. 2, and a measurement diagram is provided in Fig. 3. The working medium was heated using thermal oil.

The thermal oil was heated using a two-module electrical system. Only one module was used in the study. The heating device is a prototype unit made to special order, with a maximum power of 24 kW$_e$ per module. According to the manufacturer (Table 3), the measurement limit error for the electrical power of a single 24 kW$_e$ module is ±0.12 kW$_e$. The heating power could be adjusted in increments of 0.1 kW$_e$. The heat source was equipped with a PID controller (proportional–integral–derivative controller), which enabled the oil heating temperature to be set up to 400°C in increments of 0.1°C. The flow rates of the working fluids (thermal oil, HFE-7100 and a 40% ethylene glycol solution) were controlled using inverters mounted on the drives of the circulating pumps.

During the heating stage, the working medium was directed from the evaporator via a bypass (Fig. 3) directly to the regenerator, and then to the condenser. From the condenser, the medium

Table 3. List of measurement apparatus.

Instrument	Type/ Model	Range	Accuracy
Coriolis mass flowmeter (Siemens)	Sitrans FC Mas-sflo Mass 2100	0–5600 kg/h	±0.1%
Thermocouple (tolerance class 1, CZAKI Thermo-Product)	K-type	-40–600 ºC	±1.5ºC[A]
Pressure transducer (Trafag)	NAH 8253	0–1600 kPa(a)	±0.15%[B]
Pressure transducer (Trafag)	NAH 8253	0–400 kPa(a)	±0.15%[B]
Rotational speed measurement system – a prototype design (based on electromagnetic induction) that was ordered and subsequently manufactured	M1 TG-3	0–300 Hz	±1 rpm
Electrical power measurement system – a prototype design that was ordered and subsequently manufactured	M2 TG-3	0–16 A_{DC} 0–300 V_{DC} 0–2×24 kW	±0.5%[B] ±0.5%[B] ±0.5% (of the power)

[A] – the maximum measurement error of the thermocouple, according to the PN-EN 60584 standard.
[B] – full scale (of the measuring range).

is directed to a tank that supplies the circulating pump. The working medium pump supplies the regenerator, where the HFE-7100 fluid is preheated before being directed to the evaporator. Heat from the condenser was dissipated to the outside by means of a 50 kW_t fan cooler. In the second stage, once the working medium had reached the required pressure at the set flow rate, the HFE-7100 fluid was directed to the scroll expander inlet. The scroll expander was connected to the generator using a clutch, forming an expansion unit. The generator was loaded using a resistive load system, which consisted of 10 DC bulbs, each with a rated power of 200 W_e, connected in parallel. The load of a generator was varied by disconnecting or connecting the bulbs using switches fitted to each one. Hence, the generator was loaded using electrical receivers (light bulbs) ranging from 200 W_e to 2000 W_e. A list of control and measurement instruments, as well as sensors mounted on the test rig, is presented in Table 3.

The uncertainty of the electrical power output of the ORC system (after the AC/DC frequency converter, which converts an alternating current input voltage to a direct current output voltage) was calculated using the square error propagation rule from the following relationship:

$$\delta N_e = \sqrt{\left(\left|\frac{\delta N_e}{\delta u}\right| \delta u\right)^2 + \left(\left|\frac{\delta N_e}{\delta i}\right| \delta i\right)^2}, \quad (1)$$

where u is voltage and i represents current. The output power of the ORC system was calculated using the following relationship:

$$N_e = UI, \quad (2)$$

where U is the DC voltage and I is the current measured after the AC/DC converter.

Based on Table 3, the limit (maximum) errors of DC voltage and current measurements were estimated to be ±1.5 V and ±0.08 A, respectively. For a nominal power of the scroll expander of 1 kW (Table 1) and a maximum voltage at the generator terminals of 240 V (Table 1), the load current is 4.17 A, and the uncertainty of the electrical output power of the ORC system, determined from Eq. (1), is 1000 ± 20.2 W_e. In contrast, at the maximum power of the scroll expander of 1 kW and the maximum load current of the generator of 10 A (Table 3), the voltage is 100 V, and the uncertainty in determining the output power of the ORC system is 1000 ± 17.0 W_e.

3. Research procedures and methodology

In the first stage of the tests, the preset thermal power and the flow rate of the HFE-7100 working fluid were adjusted (e.g. 10 kW_t and 30 g/s). Next, the working fluid was directed through the bypass (with the EV valve open and the E1 and E2 valves closed), as shown in Fig. 3. It circulated within the cycle without an expander until the ORC system reached stable operating parameters (i.e. temperature and pressure). The tests were conducted at five heat source power levels (i.e. from 10 kW_t to 18 kW_t) and for HFE-7100 flow rates ranging from 30 g/s to 60 g/s (Fig. 4).

Once stable operating parameters were reached, the second stage of operation began: the EV valve was closed and the E1 and E2 valves were opened. The working fluid was then directed

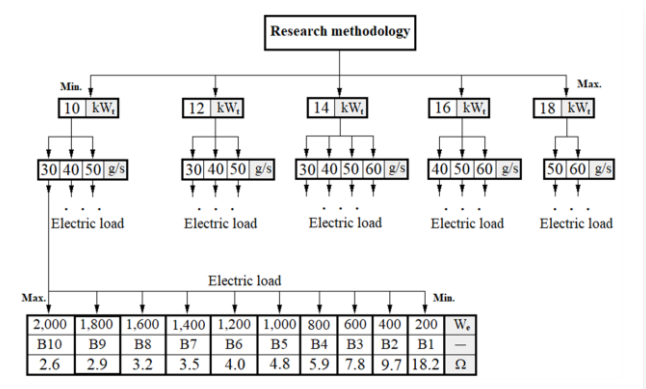

Fig. 4. Research procedure used for the scroll expander.

to the scroll expander inlet. During the start-up of the expansion unit, the generator was always loaded with energy receivers with a maximum power of 2000 W_e (i.e. ten light bulbs). The preset parameters (settings) for heat source power, generator load and working fluid flow rate were maintained at a constant level throughout the entire measurement series. Then, at a constant/preset heat source power level and HFE-7100 flow rate, the generator load was gradually reduced in steps of 200 W. This procedure was repeated until the minimum load of the expander unit's generator, 200 W, was reached. Then, with the heat source power kept constant, the flow rate was increased according to Fig. 2 (e.g. 10 kW_t and 40 g/s), and the procedure was continued until the maximum HFE-7100 flow rate was reached at the preset power level. This research procedure was applied for each thermal power level of the heat source until the maximum settings were reached, i.e. a thermal power of 18 kW_t and an HFE-7100 flow rate of 60 g/s.

4. Results and discussion

The performance characteristics of the expansion unit, illustrating the influence of the scroll expander's rotational speed on the operation of the ORC system, are presented in Sec. 4.1. The current-voltage characteristics, on the other hand, are demonstrated in Section 4.2.

4.1. Effect of the scroll expander's rotational speed

It can be seen from Fig. 5 that, at a constant thermal power of 10 kW_t for each preset and constant HFE-7100 flow rate, there is an optimum rotational speed of the scroll expander at which the electrical output power is maximised.

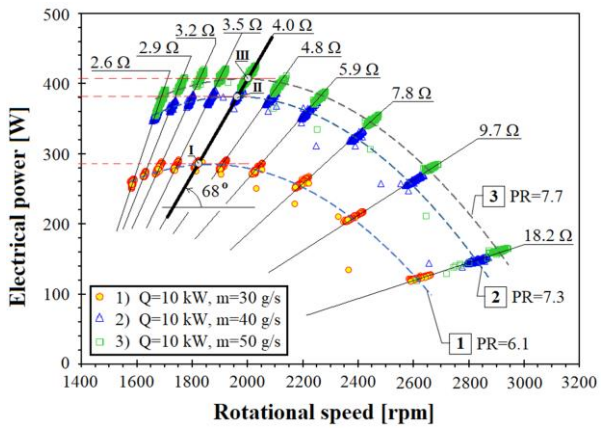

Fig. 5. Effect of the scroll expander's rotational speed on electrical power for a heat source power of 10 kW_t.

For a thermal power of 10 kW_t, the optimum rotational speed values for flow rates of 30 g/s, 40 g/s and 50 g/s were 1820 rpm, 1960 rpm and 2000 rpm, respectively. In contrast, the maximum electrical output powers of the ORC system were 282 W_e (marked as I), 390 W_e (marked as II), and 406 W_e (marked as III), respectively. By connecting points I, II and III, the optimal load line (in terms of maximum electrical power) was obtained, inclined at approximately 68° to the rotational speed axis.

The same methodology for determining the optimal load line was applied to the cases analysed below. The study found that an increase in the flow rate of the low-boiling fluid from 30 g/s to 40 g/s, i.e. by 33.3%, resulted in increases in PR and electrical output power of 19.7% and 38.3%, respectively. In contrast, the increase in HFE-7100 flow rate from 30 g/s to 50 g/s, i.e. by 66.7%, resulted in increases in PR and electrical power of 26.2% and 44%, respectively.

On the other hand, it can be seen that, irrespective of the working fluid flow rate, the voltage at the generator terminals increased linearly with the rising rotational speed of the scroll expander (Fig. 6). It was found that the inclination angle of the voltage line at the generator terminals was approximately 20°.

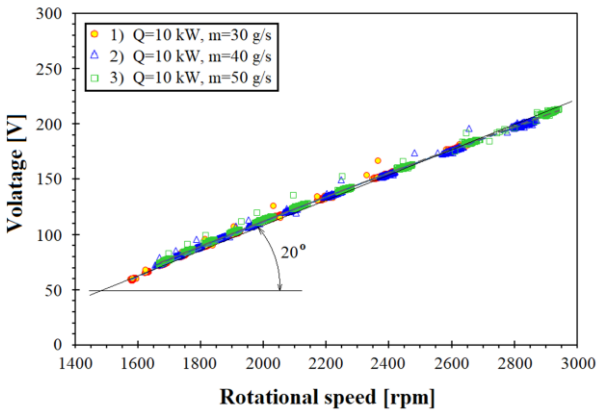

Fig. 6. Effect of the scroll expander's rotational speed on voltage at the generator terminals for a heat source power of 10 kW_t.

When the power of a heat source was 12 kW_t (Fig. 7), electrical power maxima of 282 W_e, 420 W_e and 480 W_e were obtained for HFE-7100 flow rates of 30 g/s, 40 g/s and 50 g/s, respectively. In contrast, power maxima were recorded at the expander rotational speeds of 1920 rpm, 2020 rpm and 2070 rpm, respectively. This means that as the HFE-7100 flow rate increased, both the electrical output power and the expander's rotational speed increased. The electrical power maxima lie on the load line, which has an inclination angle of approximately 75°

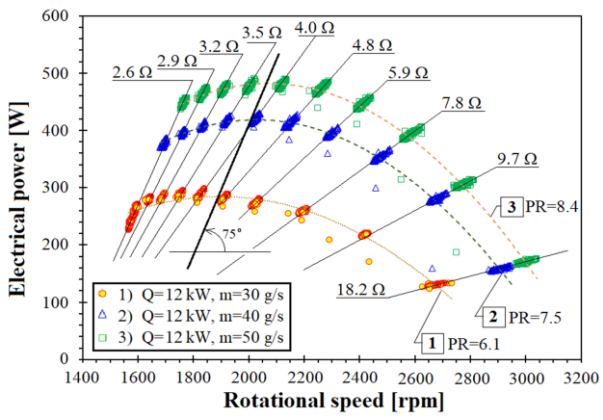

Fig. 7. Effect of the scroll expander's rotational speed on electrical power at the generator terminals for a heat source power of 12 kW_t.

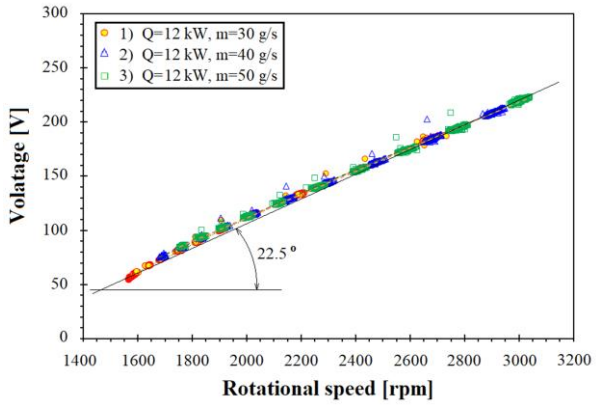

Fig. 8. Effect of the scroll expander's rotational speed on voltage at the generator terminals for a heat source power of 12 kW_t.

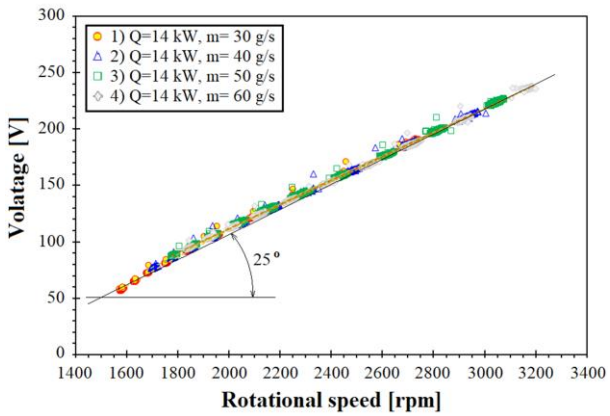

Fig. 10. Effect of the scroll expander's rotational speed on voltage at the generator terminals for a heat source power of 14 kW_t.

relative to the expander's rotational speed axis. This signifies that the inclination angle of the line representing the voltage dependence on rotational speed for a heat source power of 12 kW_t has increased compared to that for 10 kW_t by approximately 10.3%. Additionally, it was observed that the line representing the voltage dependence on rotational speed has an inclination angle of 22.5° (Fig. 8). Thus, the inclination angle of the line representing the voltage dependence on rotational speed for a heat source power of 12 kW_t, relative to that of the line obtained for a heat source power of 10 kW_t, has increased by approximately 12.5%. Meanwhile, the increase in thermal power from 10 kW_t to 12 kW_t was 20%. In contrast, the increases in electrical power at the same working fluid flow rates — i.e. 30 g/s, 40 g/s and 50 g/s — were 0%, 7.8% and 18%, respectively. This means that, as the thermal power and HFE-7100 flow rate increase, the energy losses in the ORC system decrease. Thus, for a given thermal power of the heat source, there is an optimum value of the working medium flow rate and the generator load of the scroll expander at which the electrical output power of the ORC system is maximised.

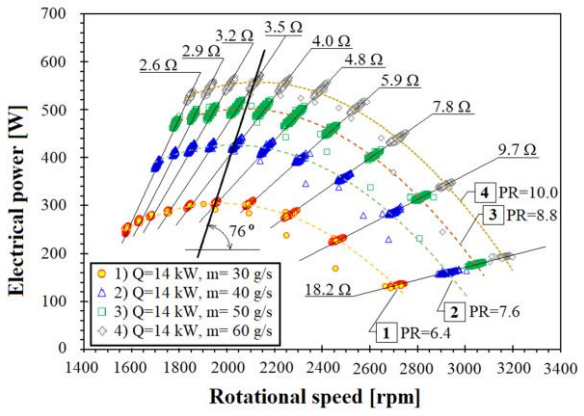

Fig. 9. Effect of the scroll expander's rotational speed on electrical power for a heat source power of 14 kW_t.

For a thermal power of 14 kW_t, an increase in the flow rate of the working medium resulted in an increase in PR and the electrical output power of the ORC system (Fig. 9). The maximum electrical powers for HFE-7100 flow rates of 30 g/s, 40 g/s, 50 g/s and 60 g/s were 304 W_e, 426 W_e, 502 W_e and 560 W_e, respectively. The electrical power maxima lie on the load line, which forms an inclination angle of approximately 76° with the expander's rotational speed axis. Consequently, the inclination angle of the load line with respect to the expander speed axis increased by approximately 11.8% compared to that at a heat source power of 10 kW_t, with a 40% increase in working medium flow rate. In contrast, the inclination angle of the voltage line with respect to the rotational speed axis increased by 25%, from 20° to 25° (Fig. 10). Hence, for the same working medium flow rate, as the thermal power of the heat source increases, higher voltages can be obtained at the generator terminals for the same rotational speed of the scroll expander.

When the power of the heat source was 16 kW_t, compared to the base power source (i.e. 10 kW_t), there was an increase in the inclination angle of the load line (Fig. 11) and in the inclination angle of the line representing the voltage at the generator terminals (Fig. 12) with respect to the expander's rotational speed axis, of approximately 13.2% and 30%, respectively. As a result, for the same HFE-7100 flow rates, an increase in the rotational

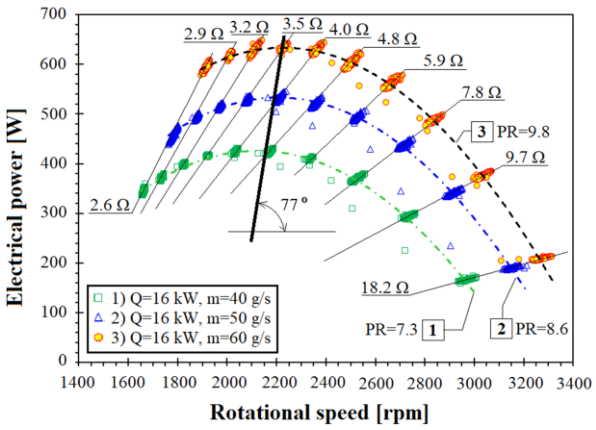

Fig. 11. Effect of the scroll expander's rotational speed on electrical power for a heat source power of 16 kW_t.

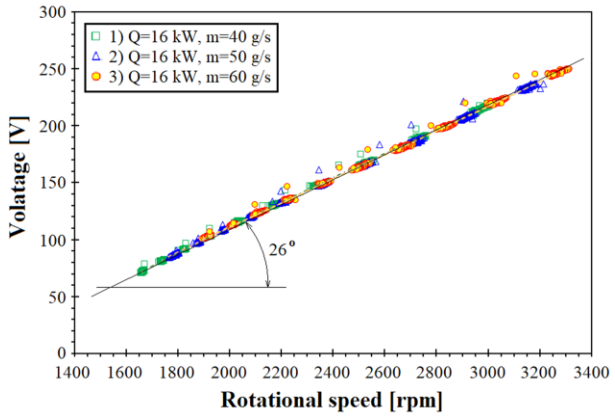

Fig. 12. Effect of the scroll expander's rotational speed on voltage at the generator terminals for a heat source power of 16 kW_t.

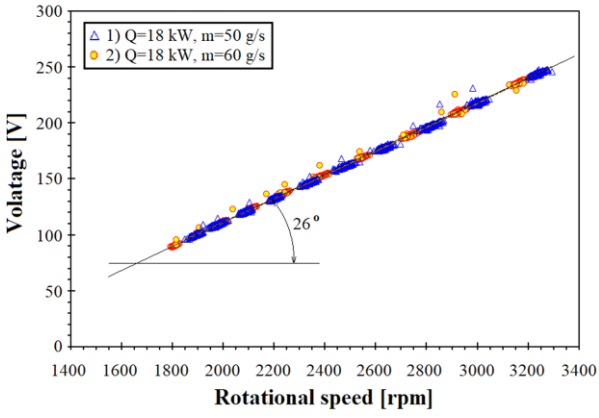

Fig. 14. Effect of the scroll expander's rotational speed on voltage at the generator terminals for a heat source power of 18 kW_t.

speed of the expander was noted, along with an increase in the electrical output power of the ORC system, as the power of the heat source increased. For example, at a flow rate of 50 g/s, the increase in the rotational speed of the expander was approximately 9.5%, and the increase in electrical power was about 32%. It is worth noting that at an HFE-7100 flow rate of 40 g/s, the increase in rotational speed with respect to the base heat source for maximum electrical power was approximately 9.2%, with speeds being 2140 rpm and 2190 rpm, respectively. In contrast, the increase in electrical power was approximately 8.7%. Since the rotational speeds of the expander were similar at flow rates of 40 g/s and 50 g/s, it can be assumed that they had little effect on the electrical output power of the system. Thus, an increase in electrical power was a direct result of the generator load current. At a heat source power of 18 kW_t, it was noted that for a low-boiling fluid flow rate of 60 g/s, the maximum electrical output power was approximately 620 W_e (Fig. 13), while at a heat source power of 16 kW_t, it was approximately 635 W_e, i.e. 2.4% higher (Fig. 11).

It was observed that the inclination angle of the line representing the voltage at the generator terminals with respect to the rotational speed was the same for heat source powers of 16 kW_t and 18 kW_t, i.e. approximately 26° (Fig. 14). Similarly, the rotational speeds of the expander were nearly identical — approximately 2190 rpm in both cases. It is noteworthy, however, that the inclination angle of the line representing the electrical power with respect to the expander's rotational speed axis was 85°, which was approximately 10.4% greater than in the case where the heat source power was 16 kW_t. Therefore, it follows from the above that for any given value of the working fluid flow rate, there is an optimum heat source power at which the electrical output power of the ORC system is maximised.

In summary, it should be noted that, irrespective of the working fluid flow rate, the inclination angles of lines representing electrical power and voltage with respect to the expander's rotational speed axis increased as the thermal power of the heat source increased.

4.2. Effect of the generator electrical load

It can be seen from Figs. 15 and 16 that the maximum electrical output powers of the system for HFE-7100 flow rates of 30 g/s, 40 g/s and 50 g/s were obtained at electric currents of approximately 3.2 A, 3.6 A and 3.7 A, respectively. For a heat source power of 10 kW_t, the inclination angle of the line representing

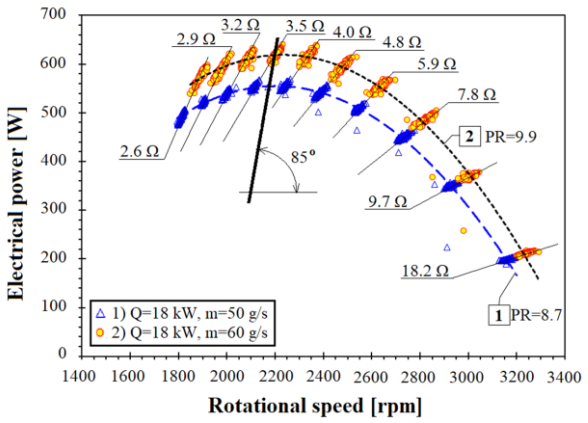

Fig. 13. Effect of the scroll expander's rotational speed on electrical power for a heat source power of 18 kW_t.

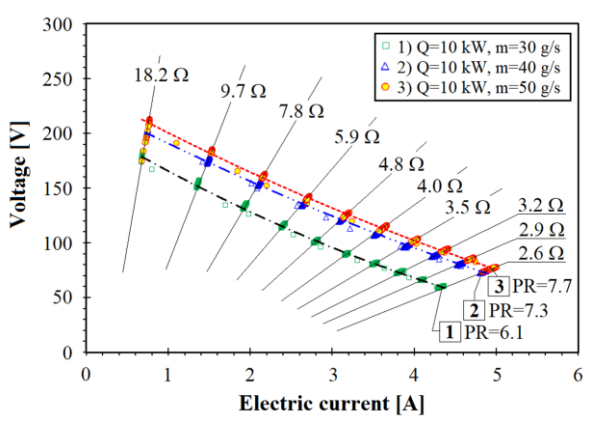

Fig. 15. Effect of electric current on the voltage at the generator terminals for a heat source power of 10 kW_t.

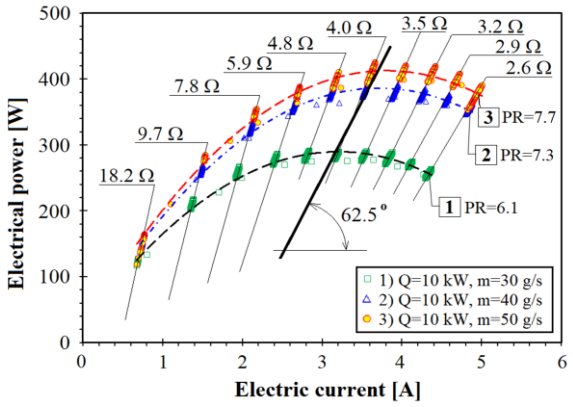

Fig. 16. Effect of electric current on the electrical output power of the ORC system for a heat source power of 10 kW_t.

electrical power versus generator load current was approximately 62.5° (Fig. 16). On the other hand, the voltage-current characteristic curve (Fig. 15) shows that, for a thermal power of 10 kW_t, the optimum generator load at which the electrical power was maximised ranged from 3.8 Ω to 4.0 Ω.

For a power of 12 kW_t, the inclination angle of the line representing the maximum electrical power with respect to the generator load current was approximately 60° (Fig. 17), which was about 4% smaller than the angle obtained for the case with a heat source power of 10 kW_t. It was observed that, for a working fluid flow rate of 30 g/s, when the thermal power was increased from 10 kW_t to 12 kW_t, the electric currents at maximum electrical power remained the same. In contrast, for 40 g/s and 50 g/s, the electric currents obtained at 12 kW_t were higher than those for a heat source power of 10 kW_t by 2.8% and 8.1%, respectively (Fig. 18). The research indicates that the optimum generator load for maximum electrical power was in the range of 3.8 Ω to 4.0 Ω.

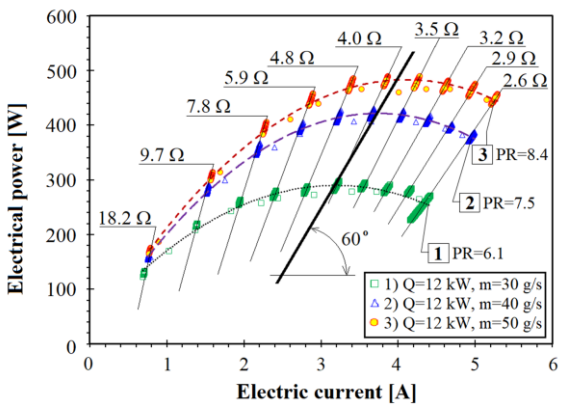

Fig. 17. Effect of electric current on the electrical output power of the ORC system for a heat source power of 12 kW_t.

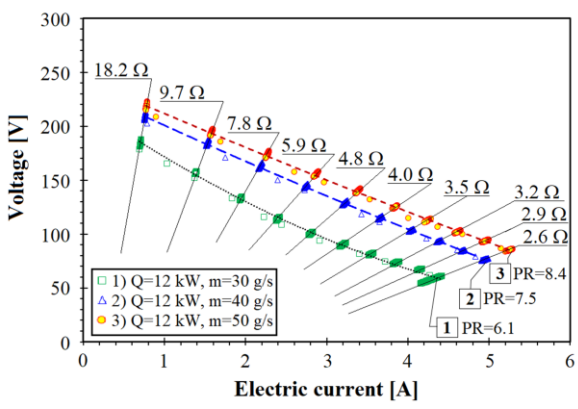

Fig. 18. Effect of electric current on the voltage at the generator terminals for a heat source power of 12 kW_t.

When the power of the heat source was 14 kW_t, the inclination angle of the line representing the maximum electrical power with respect to the generator load current was approximately 45° (Fig. 19), which was about 28% smaller than the angle obtained for a heat source power of 10 kW_t.

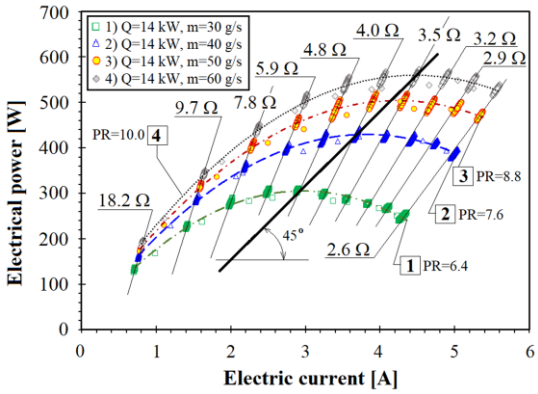

Fig. 19. Effect of electric current on the electrical output power of the ORC system for a heat source power of 14 kW_t.

In contrast, the generator load currents for HFE-7100 flow rates of 40 g/s and 50 g/s were 2.8% and 10.8% higher, respectively, than those obtained at a power of 10 kW_t (Fig. 20). At a flow rate of 30 g/s, the electric current was approximately 9.4% lower. The research showed that, with a heat source power of 14 kW_t, the optimum generator load value was in the range of 3.5 Ω to 4.7 Ω.

The research indicates that an increase in the power of the heat source from 10 kW_t to 16 kW_t resulted in a 32% decrease

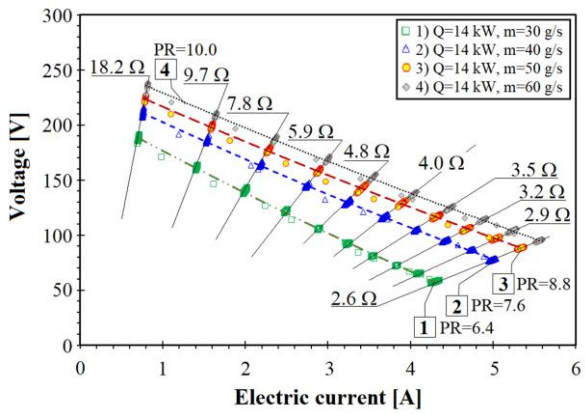

Fig. 20. Effect of electric current on the voltage at the generator terminals for a heat source power of 14 kW_t.

in the inclination angle of the line representing electrical power with respect to the electric current axis, compared to the angle obtained with a heat source power of 10 kW_t (Fig. 21).

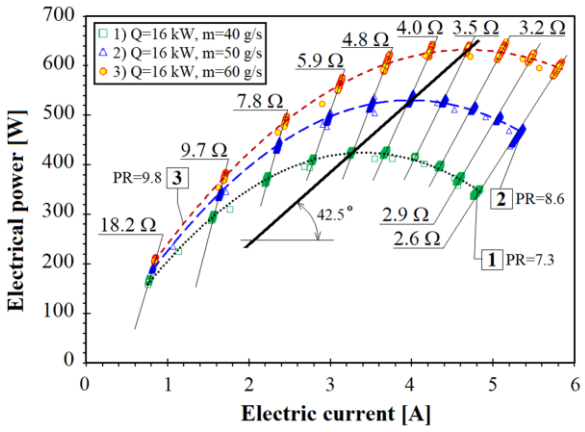

Fig. 21. Effect of electric current on the electrical output power of the ORC system for a heat source power of 16 kW_t.

At a flow rate of 40 g/s, a decrease of approximately 8.3% in the electric current was noted compared to the heat source power of 10 kW_t. Whereas, for an HFE-7100 flow rate of 50 g/s, the increase in the electric current was approximately 8.1%. It was found that the optimum load values for maximum electrical power were in the range of 3.5 Ω to 4.8 Ω (Fig. 22).

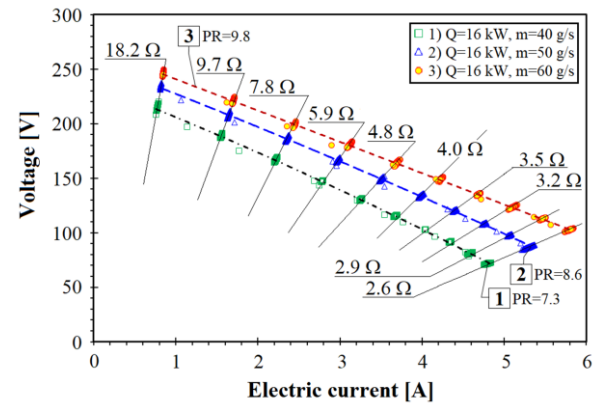

Fig. 22. Effect of electric current on the voltage at the generator terminals for a heat source power of 16 kW_t.

For a flow rate of 50 g/s and a heat source power of 18 kW_t (Fig. 23), an increase in the load current was the same, i.e. by 8.1%, as for a heat source power of 16 kW_t, compared to the base power (10 kW_t). In contrast, the inclination angle of the line representing electrical power with respect to the electric current axis was 56% smaller compared to the angle recorded for a heat source power of 10 kW_t. The research indicates that the load current of the expander generator was in the range of 3.6 Ω to 4.0 Ω (Fig. 24).

Summarising the above, it can be concluded that for the heat source powers and HFE-7100 flow rates in the ranges of 10 kW_t to 18 kWt and 30 g/s to 60 g/s, respectively, the scroll expander's generator load should be in the range of 3.5 Ω to 4.8 Ω (Table 4).

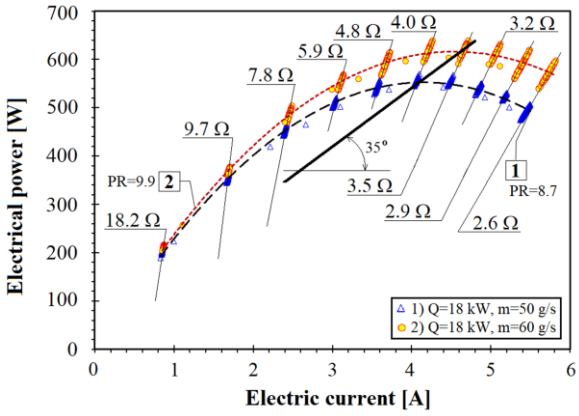

Fig. 23. Effect of electric current on the electrical output power of the ORC system for a heat source power of 18 kW_t.

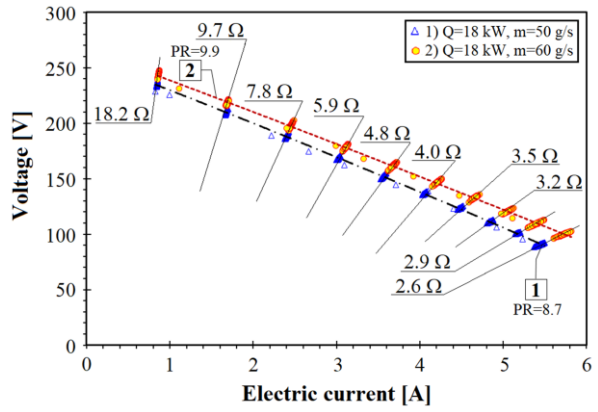

Fig. 24. Effect of electric current on the electrical output power of the ORC system for a heat source power of 18 kW_t.

Table 4. Summary of the test results for the system's maximum electrical output.

N_t (kW_t)	m (g/s)	N_e (kW_e)	PR_{av} (–)	n (rpm)	U (V)	I (A)	R_{opt} (Ω)
10	30	282	6.1	1820	90	3.2	3.8–4.0
	40	390	7.3	1960	106	3.6	
	50	406	7.7	2000	110	3.7	
12	30	282	6.1	1920	90	3.2	3.8–4.0
	40	420	7.5	2020	113	3.7	
	50	480	8.4	2070	122	4.0	
14	30	304	6.4	1990	103	2.9	3.5–4.7
	40	426	7.6	2050	113	3.7	
	50	502	8.8	2090	120	4.1	
	60	560	10.0	2120	125	4.5	
16	40	424	7.3	2140	130	3.3	3.5–4.8
	50	536	8.6	2190	135	4.0	
	60	635	9.8	2230	135	4.7	
18	50	558	8.7	2190	135	4.1	3.6–4.0
	60	620	9.9	2200	135	4.6	

5. Conclusions

The study indicates that for each value of thermal power and HFE-7100 flow rate, there is an optimum rotational speed of the scroll expander at which the electrical output power of the organic Rankine cycle (ORC) power system is maximised. In the research conducted, a maximum power of 635 W_e was obtained for a heat source power of 16 kW_t and a working fluid flow rate of 60 g/s.

It was found that, at the same working fluid flow rate, an increase in the thermal power of the heat source causes an increase in the voltage at the generator terminals for the same rotational speed. Consequently, at the same HFE-7100 flow rates, an increase in heat source power results in an increase in the electrical output power of the ORC system. Therefore, irrespective of the working medium flow rate, the inclination angles of the lines representing electrical power and voltage with respect to the expander's rotational speed axis increased as the thermal power of the heat source increased. Moreover, it was observed that, for each level of thermal power, there is an optimum generator load at which the electrical output power of the system is maximised.

Acknowledgements

This research was conducted as part of the project entitled ''Preliminary Studies of Thermodynamic Cycles Using the Low-Boiling Fluid 73DE'' (2023/07/X/ST8/01193), funded by the National Science Centre in Poland.

References

[1] Pesyridis, A., Alshammari, A.S., & Alzamil, A. (2025). Advanced energy conversion strategies using multistage radial turbines in organic Rankine cycles for low-grade heat recovery. *Case Studies in Thermal Engineering*, 69, 106034. doi: 10.1016/j.csite.2025.106034

[2] Montazerinejad, H., & Eicker, U. (2022). Recent development of heat and power generation using renewable fuels: A comprehensive review. *Renewable and Sustainable Energy Reviews*, 165, 112578. doi: 10.1016/j.rser.2022.112578

[3] Pielecha, I., & Szwajca, F. (2024). Experimental study and modelling of an air-cooled proton exchange membrane fuel cell stack in the static and dynamic performance. *Eksploatacja i Niezawodność – Maintenance and Reliability*, 26(2), 184232. doi: 10.17531/ein/184232

[4] Gunawan, G., Permana, D.I., & Soetikno, P. (2023). Design and numerical simulation of radial inflow turbine of the regenerative Brayton cycle using supercritical carbon dioxide. *Results in Engineering*, 17, 100931. doi: 10.1016/j.rineng.2023.100931

[5] Weerakoon, A.H.S., & Assadi, M. (2024). Generalized framework for micro gas turbine techno-economic assessment. *Energy Conversion and Management*, 316, 118820. doi: 10.1016/j.enconman.2024.118820

[6] Weerakoon, A.H.S., & Assadi, M. (2023). Trends and advances in micro gas turbine technology for sustainable energy solutions: A detailed review. *Energy Conversion and Management: X*, 20, 100483. doi: 10.1016/j.ecmx.2023.100483

[7] Krajewska, P., Dawidowicz, B., & Cieśliński, J.T. (2025). A concept of a micro-polygeneration system for zero-energy building. *Acta Mechanica et Automatica*, 19(1), 26−31. doi: 10.2478/ama-2025-0004

[8] Zhen, K., Shi, L., Zhang, Y., & Peng, B. (2024). Performance prediction and regression analysis of scroll expander based on response surface methodology. *Case Studies in Thermal Engineering*, 60, 104766. doi: 10.1016/j.csite.2024.104766

[9] Feng, Y.-Q., Wu, Y.-Z., Zhang, Q., Liu, Z.-N., Wang, X.-X., Hung, T.-Ch., Yu, H.-S., & He, Z.-X. (2025). Experiment investigation and machine learning prediction of a biomass-fired organic Rankine cycle combined heating and power system under various heat source temperatures and mass flow rates. *Energy*, 324, 135841. doi: 10.1016/j.energy.2025.135841

[10] Li, J., Gurgenci, H., Guan, Z., Li, J., Li, L., & Xue, Y. (2022). Multi-objective optimization of a small scale SCO_2 turbine rotor system with a shaft cooler. *Mechanics & Industry*, 23, 21. doi: 10.1051/meca/2022018

[11] Zhang, H.-H., Zhang, Y.-F., Feng, Y.-Q., Chang, J.-Ch., Chang, Ch.-W., Xi, H., Gong, L., Hung, T.-Ch., & Li, M.-J. (2023). The parametric analysis on the system behaviors with scroll expanders employed in the ORC system: An experimental comparison. *Energy*, 268, 126713. doi: 10.1016/j.energy.2023.126713

[12] Li, X., Lv, D., & Liu, Y. (2025). Optimization of organic Rankine cycle turbine expander based on radial basis function neural network and nondominated sorting genetic algorithm II. *Physics of Fluids*, 37, 035167. doi: 10.1063/5.0257260

[13] Serafino, A., Obert, B., & Cinnella, P. (2023). Multi-fidelity robust design optimization of an ORC turbine for high temperature waste heat recovery. *Energy*, 269, 126538. doi: 10.1016/j.energy.2022.126538

[14] Zhang, X., Wang, X., Cai, J., Wang, F., Bian, X., He, Z., & Tian, H. (2023). Operation strategy of a multi-mode Organic Rankine cycle system for waste heat recovery from engine cooling water. *Energy*, 263, 125934. doi: 10.1016/j.energy.2022.125934

[15] Daniarta, S., Imre, A.R., & Kolasiński, P. (2022). Thermodynamic efficiency of subcritical and transcritical power cycles utilizing selected ACZ working fluids. *Energy*, 254(A), 124432. doi: 10.1016/j.energy.2022.124432

[16] Belousov, A.E., & Ovchinnikov, E.S. (2022). Mathematical modeling of the operation of an expander-generator pressure regulator in non-stationary conditions of small gas pressure reduction stations. *Mathematics*, 10(3), 393. doi: 10.3390/math10030393

[17] Kruk-Gotzman, S., Ziółkowski, P., Iliev, I., Negreanu, G.-P., & Badur, J. (2023). Techno-economic evaluation of combined cycle gas turbine and a diabatic compressed air energy storage integration concept. *Energy*, 266, 126345. doi: 10.1016/j.energy.2022.126345

[18] Guan, Y., Li, W., Zhu, Y., Wang, X., Zhang, Y., & Chen, H. (2024). Energy loss analysis in two-stage turbine of compressed air energy storage system: Effect of varying partial admission ratio and inlet pressure. *Energy*, 305, 132214. doi: 10.1016/j.energy.2024.132214

[19] Kolasiński, P., & Daniarta, S. (2021). Sizing the thermal energy storage (TES) device for organic Rankine cycle (ORC) power systems. *MATEC Web of Conferences*, 345, 00018. doi: 10.1051/matecconf/202134500018

[20] Tauveron, N., Lhermet, G., Payebien, B., Caney, N., & Morin, F. (2024). an experimental study of an autonomous heat removal system based on an organic Rankine cycle for an advanced nuclear power plant. *Energies*, 17(20), 5069. doi: 10.3390/en17205069

[21] González, J., Llovell, F., Garrido, J.M., & Quinteros-Lama, H. (2023). A study of the optimal conditions for organic Rankine cycles coupled with vapour compression refrigeration using a rigorous approach based on the Helmholtz energy function. *Energy*, 285, 129554. doi: 10.1016/j.energy.2023.129554

[22] Hasan, A., Mugdadi, B., Al-Nimr, M.A., & Tashtoush, B. (2022). Direct and indirect utilization of thermal energy for cooling generation: A comparative analysis. *Energy*, 238(C), 122046. doi: 10.1016/j.energy.2021.122046

[23] Ahmed, A.M. (2024). Thermal efficiency investigation for organic Rankine cycle and trilateral flash cycle using hydrofluoroether working fluids. *Results in Engineering*, 21, 101648. doi: 10.1016/j.rineng.2023.101648

[24] Ahmed, A.M. (2022). Assessment of the thermal efficiency of subcritical power generation cycles using environmentally friendly fluids at various heat source temperatures. *Energy Science & Engineering*, 10(12), 4768−4781. doi: 10.1002/ese3.1307

[25] Witanowski, Ł. (2024). Multi-objective optimization of a small-scale ORC-VCC system using low-GWP refrigerants. *Energies*, 17(21), 5381. doi: 10.3390/en17215381

[26] Sanaye, S., & Ghaffari, A. (2023). Transient modeling and thermal analysis of an innovative dual-loop Rankine–organic Rankine heat recovery system integrated with a gas engine. *Journal of Thermal Analysis and Calorimetry*, 148, 10951−10971. doi: 10.1007/s10973-023-12435-3

[27] Di Battista, D., & Cipollone, R. (2023). Waste energy recovery and valorization in internal combustion engines for transportation. *Energies*, 16(8), 3503. doi: 10.3390/en16083503

[28] Kupka, D., Koloničný, J., & Pejchal, J. (2025). Development of an axial impulse turbine for a small-scale ORC system. *Results in Engineering*, 25, 103994. doi: 10.1016/j.rineng.2025.103994

[29] Feng, Y.-Q., Xu, K.-J., Liu, Z.-X., Yu, H.-S., Hung, T.-Ch., & He, Z.-X. (2024). Construction and preliminary test of a biomass-fired organic Rankine cycle system for heat and power system. *Energy*, 308, 133021. doi: 10.1016/j.energy.2024.133021

[30] Abdalhamid, A.M.K., & Eltaweel, A. (2024). Design and analysis of a single-stage supersonic turbine with partial admission. *Energy*, 309, 133100. doi: 10.1016/j.energy.2024.133100

[31] Hossain, M.S., Sultan, I., Phung, T., & Kumar, A. (2024). An optimum design for a fast-response solenoid valve: Application to a limaçon gas expander. *Dynamics*, 4(2), 457−474. doi: 10.3390/dynamics4020024

[32] Zaniewski, D., Klimaszewski, P., Klonowicz, P., Witanowski, Ł., Lampart, P., Jędrzejewski, Ł., & Suchocki, T. (2023). Organic Rankine cycle turbogenerator cooling – Optimization of the generator water jacket heat exchange surface. *Applied Thermal Engineering*, 223, 120041. doi: 10.1016/j.applthermaleng.2023.120041

[33] Ma, C., Yang, Q., Sun, X., Zhang, K., & Li, L. (2022). Performance analysis of externally pressurized gas journal bearing lubricated with vapor of R134a in centrifugal compressor. *Processes*, 10(10), 2067. doi: 10.3390/pr10102067

[34] Kaczmarczyk, T.Z., & Żywica, G. (2024). Experimental study of the effect of load and rotational speed on the electrical power of a high-speed ORC microturbogenerator. *Applied Thermal Engineering*, 238, 122012. doi: 10.1016/j.applthermaleng.2023.122012

[35] Aziz, F., Kamal, S.M., Perl, M., & Chetry, A. (2024). Increasing the load carrying capacity of hollow rotating disks by applying rotational autofrettage. *European Journal of Mechanics - A/Solids*, 105, 105231. doi: 10.1016/j.euromechsol.2024.105231

[36] Daniarta, S., Kolasiński, P., Imre, A.R., & Sowa, D. (2024). Artificial intelligence-driven performance mapping: A deep learning-based investigation of a multi-vane expander in retrofitted organic Rankine cycle. *Energy Conversion and Management*, 315, 118763. doi: 10.1016/j.enconman.2024.118763

[37] Li, Ch., Guo, Z., Guo, H., Bao, X., & Zhou, L. (2022). Influences of main design parameters on the aerodynamic performance of a micro-radial inflow turbine. *AIP Advances*, 12(10), 105012. doi: 10.1063/5.0090173

[38] Zhang, Y., Zhang, S., Peng, H., Tian, Z., Gao, W., & Yang, K. (2023). Thermodynamic analysis of Tesla turbine in organic Rankine cycle under two-phase flow conditions. *Energy Conversion and Management*, 276, 116477. doi: 10.1016/j.enconman.2022.116477

[39] Wu, T., Cai, S., Yao, Z., Yin, X., Ma, X., Gao, X., Xie, F., Yang, H., Shen, X., & Shao, L. (2024). Design and optimization of the radial inflow turbogenerator for organic Rankine cycle system based on the genetic algorithm. *Applied Thermal Engineering*, 253, 123749. doi: 10.1016/j.applthermaleng.2024.123749

[40] Witanowski, Ł., Klonowicz, P., Lampart, P., Klimaszewski, P., Suchocki, T., Jędrzejewski, Ł., Zaniewski, D., & Ziółkowski, P. (2023). Impact of rotor geometry optimization on the off-design ORC turbine performance. *Energy*, 265, 126312. doi: 10.1016/j.energy.2022.126312

[41] Wang, E., & Peng, N. (2023). A review on the preliminary design of axial and radial turbines for small-scale Organic rankine cycle. *Energies*, 16(8), 3423. doi: 10.3390/en16083423

[42] Rusanov, R., Kravchenko, I., Rusanov, A., Riznyk, S., Kukhtin, Y., Chugay, M., & Sukhanov, M. (2025). Development experience of the centripetal turbine flow part for an aviation engine air starter. *Aerospace Technic and Technology*, 1(201). doi: 10.32620/aktt.2025.1.04

[43] Peng, N., Wang, E., Meng, F., Zhang, W., Wang, Y., Zhang, B., Zhao, Y., & Yenga, E.Ch.Y. (2024). Experimental investigation on off-design performance of a small-scale two-stage counter-rotating impulse turbine. *International Journal of Energy Research*, 4623244, 21. 10.1155/2024/4623244

[44] Witanowski, Ł., Klonowicz, P., Lampart, P., & Ziółkowski, P. (2023). Multi-objective optimization of the ORC axial turbine for a waste heat recovery system working in two modes: cogeneration and condensation. *Energy*, 264, 126187. doi: 10.1016/j.energy.2022.126187

[45] Włodarski, W., & Piwowarski, M. (2024). A model modification for a microturbine set with partial admission stages. *Energies*, 17(8), 1792. doi: 10.3390/en17081792

[46] Sun, T., Liu, Y., Ma, Z., Shu, P., & Ye, Z. (2024). Numerical simulation of the relationship between steam flow excitation characteristics and coverage on the governing stage of marine steam turbine. *Ocean Engineering*, 314(1), 119526. doi: 10.1016/j.oceaneng.2024.119526

[47] Kaczmarczyk, T.Z., & Żywica, G. (2022). Experimental study of a 1 kW high-speed ORC microturbogenerator under partial load. *Energy Conversion and Management*, 272, 116381. doi: 10.1016/j.enconman.2022.116381

[48] Lu, Y., Guo, Z., Zheng, Z., Wang, W., Wang, H., Zhou, F., & Wang, X. (2023). Underwater propeller turbine blade redesign based on developed inverse design method for energy performance improvement and cavitation suppression. *Ocean Engineering*, 277, 114315. doi: 10.1016/j.oceaneng.2023.114315

[49] Witanowski, Ł., Ziółkowski, P., Klonowicz, P., & Lampart, P. (2023). A hybrid approach to optimization of radial inflow turbine with principal component analysis. *Energy*, 272, 127064. doi: 10.1016/j.energy.2023.127064

[50] Liaw, K.L., Kurnia, J.C., Lai, W.K., Ong, K.Ch., Zar, A.B.M.A., Muhammad, M.F.B., & Firmansyah. (2023). Optimization of a novel impulse gas turbine nozzle and blades design utilizing Taguchi method for micro-scale power generation. *Energy*, 282, 129018. doi: 10.1016/j.energy.2023.129018

[51] Peng, N., Wang, E., Wang, W., Lu, J., & Li, M. (2024). Aerodynamic analysis of a 1.5 kW two-stage counter-rotating partial-admission impulse turbine for small-scale power system with a high expansion pressure ratio. *Case Studies in Thermal Engineering*, 53, 103824. doi: 10.1016/j.csite.2023.103824

[52] Peng, N., Wang, E., & Wang, W. (2023). Design and analysis of a 1.5 kW single-stage partial-admission impulse turbine for low-grade energy utilization. *Energy*, 268, 126631. doi: 10.1016/j.energy.2023.126631

[53] He, S., Tong, Z., Tong, S., Chen, K., & Cao, X.E. (2025). Collaborative optimization of turbo-expander impellers and guide vanes to mitigate flow-induced vibrations. *Physics of Fluids*, 37(3), 035178. doi: 10.1063/5.0257754

[54] Mukherjee, A., & Seshadri, S. (2023). Numerical study on the effect of port geometry of intake manifold in a steam Wankel expander. *Thermal Science and Engineering Progress*, 37, 101621. doi: 10.1016/j.tsep.2022.101621

[55] Wei, J., Hua, Q., Yuan, L., Li, G., Wang, J., & Wang, J. (2023). A review of the research status of scroll expander. *Proceedings of the Institution of Mechanical Engineers, Part A: Journal of Power and Energy*, 237(1), 176−197. doi: 10.1177/09576509221109245

[56] Wołowicz, M., Kolasiński, P., & Badyda, K. (2021). Modern small and microcogeneration systems — A review. *Energies*, 14(3), 785. doi: 10.3390/en14030785

[57] Ping, X., Yang, F., Zhang, H., Wang, Y., Lei, B., & Wu, Y. (2022). Performance limits of the single screw expander in organic Rankine cycle with ensemble learning and hyperdimensional evolutionary many-objective optimization algorithm intervention. *Energy*, 245, 123254. doi: 10.1016/j.energy.2022.123254

[58] Gopal, V.V., & Seshadri, S. (2022). Effect of cut-off and compression ratio on the isentropic efficiency during off-design and part-load operations of a Wankel rotary steam expander used for small scale cogeneration. *Applied Thermal Engineering*, 207, 118212. doi: 10.1016/j.applthermaleng.2022.118212

[59] Ekwonu, M.C., Kim, M., Chen, B., Nasir, M.T., & Kim, K.C. (2023). Dynamic simulation of partial load operation of an organic Rankine cycle with two parallel expanders. *Energies*, 16(1), 519. doi: 10.3390/en16010519

[60] Kaczmarczyk, T.Z. (2021). Experimental research of a small biomass organic Rankine cycle plant with multiple scroll expanders intended for domestic use. *Energy Conversion and Management*, 244, 114437. doi: 10.1016/j.enconman.2021.114437

[61] Kaczmarczyk, T.Z. (2024). Experimental research of a pumping engine in a micro-ORC system with a low-boiling medium. *Archives of Thermodynamics*, 45(4), 125–140. doi: 10.24425/ather.2024.152002

[62] Kaczmarczyk, T.Z., Ihantowicz, E., Żywica, G., & Kaniecki, M. (2019). Experimental study of the prototype of a Roto-Jet pump for the domestic ORC power plant. *Archives of Thermodynamics*, 40(3), 83–108. doi: 10.24425/ather.2019.129995

[63] Sprouse, III C.E. (2024). Review of organic Rankine cycles for internal combustion engine waste heat recovery: Latest decade in review. *Sustainability*, 16(5), 1924. doi: 10.3390/su16051924

[64] Abbas, W.K.A., Baumhögger, E., & Vrabec, J. (2022). Experimental investigation of organic Rankine cycle performance using alkanes or hexamethyldisiloxane as a working fluid. *Energy Conversion and Management: X*. 15, 100244. doi: 10.1016/ j.ecmx.2022.100244

[65] Huo, E., Xin, L., & Wang, S. (2022). Thermal stability and pyrolysis mechanism of working fluids for organic Rankine cycle: A review. *International Journal of Energy Research*, 46, 19341–19356. doi: 10.1002/er.8518

[66] Colak, A.B., & Arslan, O. (2024). Numerical analysis-based performance assessment of the small-scale organic Rankine cycle turbine design for residential applications. *Thermal Science and Engineering Progress*, 51, 102626. doi: 10.1016/j.tsep.2024.102626

[67] Kottapallia, A., & Konijeti, R. (2022). Numerical and experimental investigation of nonlubricated air scroll expander derived from a refrigerant scroll compressor. *Frontiers in Heat and Mass Transfer*, 19(1), 1–11. doi: 10.5098/hmt.19.11

[68] Zhang, Y., Tsai, Y.-Ch., Ren, X., Tuo, Z., Wang, W., Gong, L., & Hung, T.-Ch. (2024). Experimental study of the external load characteristics on a micro-scale organic Rankine cycle system. *Energy*, 306, 132453. doi: 10.1016/j.energy.2024.132453

[69] Murthy, A.A., Norris, S., & Subiantoro, A. (2022). Performance of a four-intersecting-vane expander in a R134a refrigeration cycle. *Applied Thermal Engineering*, 209, 118244. doi: 10.1016/j.applthermaleng.2022.118244

[70] Sun, H., Li, H., Gao, P., Hou, F., Hung, T.-Ch., Chang, Y.-H., Lin, Ch.-W., & Qin, J. (2024). Numerical simulation and low speed experiment of a low partially admitted rate axial turbine for small scale organic Rankine cycle. *Applied Thermal Engineering*, 238, 122002. doi: 10.1016/j.applthermaleng.2023.122002

[71] Sun, J., & Peng, B. (2025). Experimental study on the influence of pump frequencies and oil flow rates on the performance of organic Rankine cycle systems. *Case Studies in Thermal Engineering*, 69, 106028. doi: 10.1016/j.csite.2025.106028

[72] Kaczmarczyk, T.Z., & Żywica, G. (2022). Experimental research of a micropower volumetric expander for domestic applications at constant electrical load. *Sustainable Energy Technologies and Assessments*, 49, 101755. doi: 10.1016/j.seta.2021.101755